

## Article

# Re-Os Systematics in the Layered Rocks and Cu-Ni-PGE Sulfide Ores from the Dovyren Intrusive Complex in Southern Siberia, Russia: Implications for the Original Mantle Source and the Effects of Two-Stage Crustal Contamination

Alexey A. Ariskin <sup>1,2,\*</sup>, Svetlana G. Tessalina <sup>3</sup>, Yuri A. Kostitsyn <sup>2</sup>, Ivan V. Pshenitsyn <sup>2</sup>, Sergei N. Sobolev <sup>2</sup>, Georgy S. Nikolaev <sup>2</sup> and Evgeny V. Kislov <sup>4</sup>

- <sup>1</sup> Faculty of Geology, Lomonosov Moscow State University, Leninskie Gory 1, 119234 Moscow, Russia  
<sup>2</sup> Vernadsky Institute of Geochemistry and Analytical Chemistry, Russian Academy of Sciences, Kosygin Str. 19, 119991 Moscow, Russia; kostitsyn@geokhi.ru (Y.A.K.); lotecsi@gmail.com (I.V.P.); ssn\_collection@bk.ru (S.N.S.); gsnikolaev@rambler.ru (G.S.N.)  
<sup>3</sup> John de Laeter Centre for Isotope Research, Curtin University, Kent Str., Bentley, WA 6102, Australia; svetlana.tessalina@curtin.edu.au  
<sup>4</sup> Dobretsov Geological Institute, Siberian Branch of Russian Academy of Sciences, Sakhyanovoy Str. 6a, 670047 Ulan-Ude, Russia; evg-kislov@yandex.ru  
\* Correspondence: ariskin@rambler.ru



**Citation:** Ariskin, A.A.; Tessalina, S.G.; Kostitsyn, Y.A.; Pshenitsyn, I.V.; Sobolev, S.N.; Nikolaev, G.S.; Kislov, E.V. Re-Os Systematics in the Layered Rocks and Cu-Ni-PGE Sulfide Ores from the Dovyren Intrusive Complex in Southern Siberia, Russia: Implications for the Original Mantle Source and the Effects of Two-Stage Crustal Contamination. *Minerals* **2023**, *13*, 1356. <https://doi.org/10.3390/min13111356>

Academic Editor: Maria Economou-Eliopoulos

Received: 22 August 2023  
Revised: 11 October 2023  
Accepted: 21 October 2023  
Published: 24 October 2023



**Copyright:** © 2023 by the authors. Licensee MDPI, Basel, Switzerland. This article is an open access article distributed under the terms and conditions of the Creative Commons Attribution (CC BY) license (<https://creativecommons.org/licenses/by/4.0/>).

**Abstract:** The Dovyren Intrusive Complex (Northern Baikal region,  $728 \pm 3$  Ma) includes the dunite-troctolite-gabbro-norite Yoko-Dovyren massif (YDM) associated with a sequence of underlying mafic-to-ultramafic sills, locally demonstrating interbedding relations with the most primitive rocks of the pluton. These sills and apophyses contain sulfide mineralization ranging from globular to net-textured and massive ores. Major types of the YDM cumulates and sulfide mineralization were examined for their PGE contents and Re-Os isotopic systematics. The ten analyzed samples included chilled and basal rocks, poorly mineralized troctolite, PGE-rich anorthosite, as well as three samples from a thick ore-bearing apophysis DV10 connected with the YDM. These samples yielded a Re-Os isochron with an age of  $759 \pm 36$  Ma and an initial  $^{187}\text{Os}/^{188}\text{Os}$  of  $0.1309 \pm 0.0026$  (MSWD = 110), which is in consistent with the previously reported U-Pb zircon age. It is shown that being recalculated to  $\gamma\text{Os}(t)$  at  $t = 728$  Ma, these isotopic compositions demonstrate three clusters regarding the relationship between  $\gamma\text{Os}(t)$  and  $^{187}\text{Re}/^{188}\text{Os}$ : (i) the chilled gabbro-norite (YDM) and subcontact olivine gabbro-norite (DV10) yielded the most radiogenic values of  $\gamma\text{Os}(t)$  10.5 and 10.0 among basal ultramafics, (ii) plagiodunite, troctolite, and sulfide ores showed lower radiogenic compositions, with  $\gamma\text{Os}(t)$  ranging from 7.3 to 8.7, (iii) olivine gabbro-norite, plagioperidotite, and one sample of PGE-rich anorthosite yield very primitive  $\gamma\text{Os}(t)$  in the range 4.5 to 5.6 (on average  $5.2 \pm 0.6$ ). The lowest values of  $\gamma\text{Os}(t)$  for the least fractionated rocks of the YDM suggest a primitive mantle source, formed from a partly contaminated Neoproterozoic protolith, which is considered to be anomalous in Upper Riphean due to very low  $\epsilon\text{Nd}(t)$  of  $-16$  for the most primitive Dovyren magma (Fo88-parent). The highest values of  $\gamma\text{Os}(t)$  and relative enrichment in the  $^{34}\text{S}$  isotope in the chilled gabbro-norite (YDM) and subcontact olivine gabbro-norite (DV10) evidence that their primitive to evolved magmatic precursors could be affected by a metamorphic fluid enriched in radiogenic  $^{187}\text{Os}$ , originating in the exocontact halo due to the thermal decomposition of pyrite from the dehydrated country rocks. This is consistent with the second-stage contamination of the Dovyren magma by the hosting crustal rocks (probably of 10 wt% shists), generating more evolved Fo86-parent magma with higher  $\epsilon\text{Nd}(t)$  of  $-14$ .

**Keywords:** Dovyren; sulfide ore; PGE-rich anorthosite; Re-Os isotopic system; anomalous mantle protolith; crustal contamination

## 1. Introduction

The Yoko–Dovyren layered massif (herein after YDM) is the largest intrusive body of the ~728 Ma Dovyren Intrusive Complex, which is located ~60 km NE of Lake Baikal and represents the eastern branch of the Cu-Ni-PGE East Siberian metallogenic province [1–5]. It forms a 26 km long lens-shaped ridge, which is up to ~3.5 km wide in its central part, being composed of a succession of ultramafic and mafic rocks ranging from plagioperidotite and dunite to troctolite, olivine gabbro, and gabbrobronorite. A unique feature of the regional geology is the concordance of the intrusive rocks with the enclosing carbonate–terrigenous sediments along its strike and dip, which is nearly vertical due to post-intrusive folding. This allows one to sample the YDM across the strike, from the lower to upper contacts. It seems to be one of the best-exposed layered complexes in the world and, over the last several decades, it has continued to be a reference site for Russian petrologists dealing with the Cu-Ni-PGE fertility of layered intrusions. This is because of its relatively simple geological setting, excellent exposures, and the occurrence of common types of Cu-Ni sulfide and PGE mineralization [2,5–12].

Petrological reconstructions for the basal zone in the thickest part of the YDM indicate a high-Mg S-undersaturated parental magma containing ~11 wt.% MgO and 52 wt.% SiO<sub>2</sub> at the temperature of 1285 °C, which is in equilibrium with olivine Fo<sub>87.5–88</sub> [5]. Correspondingly, most primitive rocks locally associate with relatively evolved Ol-Pl cumulates that crystallized at lower temperatures (1220–1180 °C) and originally contained olivine Fo<sub>86–84</sub>. The latter rocks are predominant in basal parts of the intrusion in the SW and NE terminations of the Dovyren Ridge, as well as composing underlying mafic-to-ultramafic sills, considered as apophyses from the main body and containing sulfide mineralization, ranging from disseminated sulfides to globular, net-textured, and massive ores.

Thermodynamic calculations with the COMAGMAT-5 model allowed quantification of the fundamental differences between specific types of the YDM protocumulate systems, including their sulfide saturation history [5,12,13]. However, many questions remain unresolved. Of key importance is the nature of the mantle source and the probable role of crustal contamination, including both prehistory of SCLM and details of magma emplacement, which could involve assimilation of host rocks. To provide insight into the scales of these processes, we performed a Sr-Nd-Pb isotope study of the YDM rocks, which demonstrated anomalously enriched isotopic compositions of Sr and Nd [4]. The maximum enrichment ( $^{87}\text{Sr}/^{86}\text{Sr}(t) = 0.71387$  and  $\epsilon\text{Nd}(t) = -16.09$ ) was found in the contact and lowermost rocks of the layered intrusion, which crystallized from the Mg magma. Most overlying rocks from the main cumulate succession proved to be less isotopically enriched with  $\epsilon\text{Nd}$  in the range from  $-14.5$  to  $-13.5$ . These data suggest a prolonged evolution of an anomalous Dovyren magma source, which could have been formed in the Neoproterozoic era during the crustal accretion of the Siberian craton.

To provide more arguments for the complex history that led to the isotopic diversity of the YDM rocks, principal types of the Dovyren cumulates and sulfide mineralization were examined for their PGE contents and Re-Os isotopic systematics.

## 2. General Structure of the YDM and Associated Bodies

### 2.1. Main Types of the Dovyren Rocks

Despite its Late Riphean age, the YDM has not been metamorphosed significantly, so most of its intrusive rocks are unaltered, preserving both their igneous textures and original mineralogy. The typical succession of contact rocks and overlying cumulates, composing the layered series of the YDM, has been described in the central part of the intrusion, along the combined Bolshoi–Tsentralnyi cross section [2,5] (Figure 1).

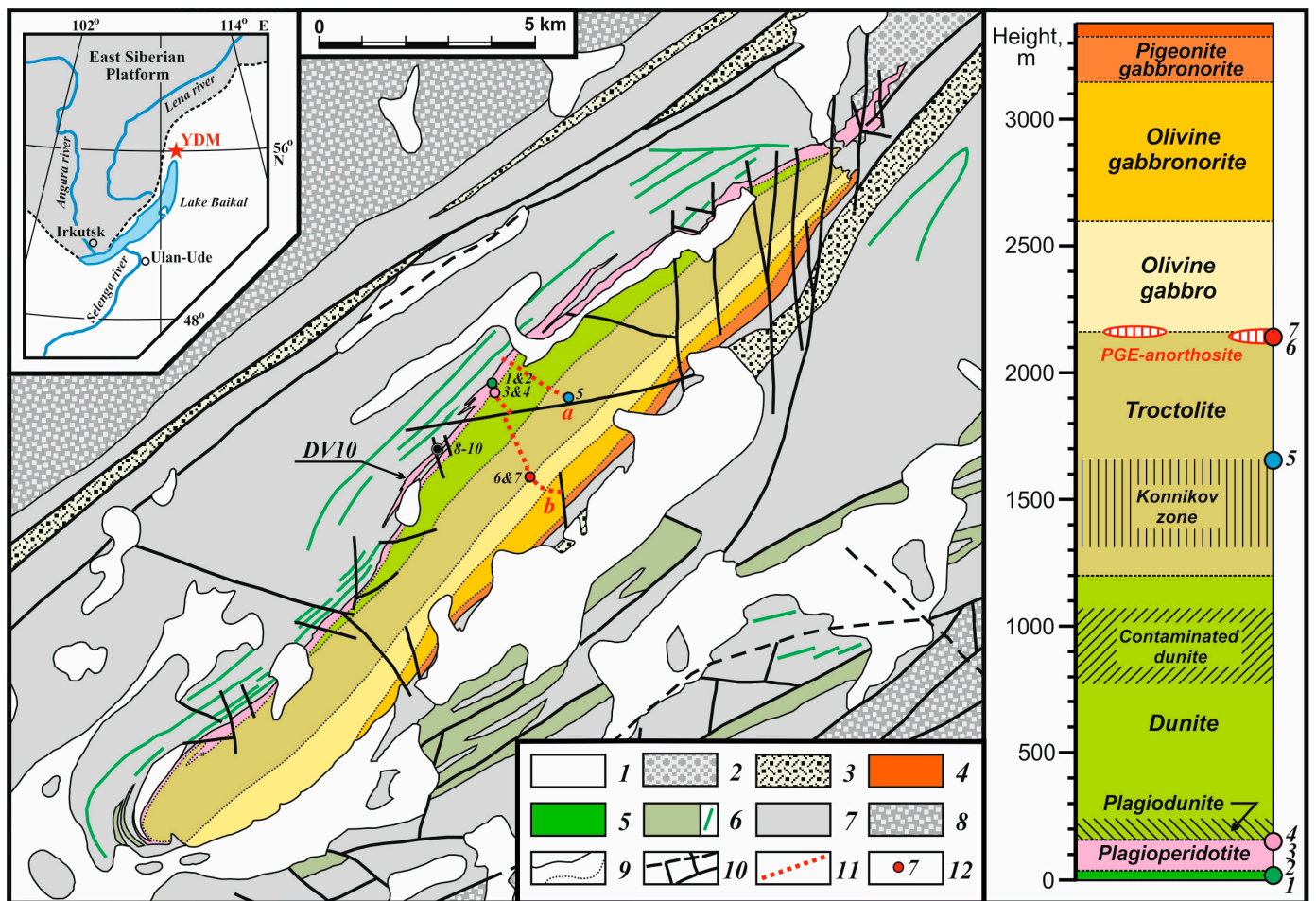


**Figure 1.** Geological map of the Dovyren area and generalized structure of the Yoko–Dovyren massif, with changes after [5]. 1, Quaternary rocks (Middle–Late Quaternary). 2, Kholodninskaya formation (Vendian–Early Cambrian). 3, The Inyaptuk suite of high-Ti basalts. 4–5, Endocontact rocks of the YDM: 4, chilled gabbronorite; 5, chilled olivine gabbronorite and picrodolerite; 6, small bodies of mafic to ultramafic rocks; 7–8, carbonate–terrigenous rocks: 7, the Synnyr rift and 8, the Olokit trough. 9, Geological boundaries. 10, Faults. 11, Main sampled cross sections: (a) Bolshoi, (b) Tsentralnyi. 12, Circles numbered 1–10 correspond to examined samples listed in Table 1. Insets show the location scheme (to the left) and main stratigraphic units of the YDM in its central part (to the right). Contaminated dunitites host numerous xenoliths of magnesian skarns. The Konnikov zone includes poorly mineralized troctolites, locally enriched in PGE minerals [11].

### 2.1.1. Chilled Gabbronorite and Picrodolerite

The lower contact between hornfels and intrusive rocks in this area includes several tens of centimeters of chilled fine-grained gabbronorite with rare phenocrysts of olivine (Figure 2a,b) followed by a 3–4 m thick zone of the so-called picrodolerite. Compositionally, both types represent olivine gabbronorite, which is composed of variable amounts of subhedral cumulus olivine enclosed in the ophitic groundmass of plagioclase and pyroxenes, with some amounts of phlogopite oikocrysts and rare grains of accessory chromite and apatite. Only rare and small interstitial grains of sulfides can be found in the chilled gabbronorite and picrodolerite.

**Table 1.** Stratigraphic position and specific features of the examined YDM rocks and Cu-Ni-PGE sulfide ores from the DV10 apophysis.

No	Sample	h, m	Lithology	CIPW, wt.%		Mineral Compositions, mol.%		S, wt.%	Cu, ppm
				OI	PI	Fo (OI)	An (PI)		
<b>Yoko–Dovyren intrusion</b>									
1	DV30-1b	0.4	Chilled olivine gabbronorite	20	39	73.3 ± 2.4	55.1 ± 7.8	0.09	70.0
2	DV30-4b	5.4	Olivine gabbronorite	47	27	83.2 ± 1.0	63.5 ± 6.3	0.06	57.0
3	13DV547-16	160	Pl-peridotite	65	13	85.5 ± 0.2	73.1 ± 4.8	0.02	28.0
4	13DV547-60	187	Poor mineralized plagioclone	83	11	85.6 ± 0.2	75.6 ± 5.1	0.06	108
5	13DV554-1	1660	PGE-mineralized troctolite	57	42	84.0 ± 0.4	87.9 ± 1.8	0.09	486
6	AA06a-1	2159	PGE-mineralized anorthosite	1	94	80.4 ± 0.4	84.4 ± 0.7	1.47	5535
7	AA06a-2		2	92	1.08			2503	
<b>Ore-bearing apophysis DV10</b>									
8	DV627-1-3	8.5	Globule-containing Ol-gabbronorite	47	24	77.1 ± 2.1	67.9 ± 3.4	0.54	676
9	DV625-2_M	13	Net-textured ore	37	6	81.7 ± 0.9	65.6 ± 7.4	11.5	3699
10	DV628-2	21	Globular ore	42	20	80.6 ± 3.2	60.2 ± 16	3.43	824

Note. All Dovyren samples, except troctolite 13DV554-1, are taken along the Bolshoi cross section used as a basic stratigraphic succession (Figure 1). The average compositions of olivine and plagioclase are calculated from EPMA analyses of 5 to 20 grains.

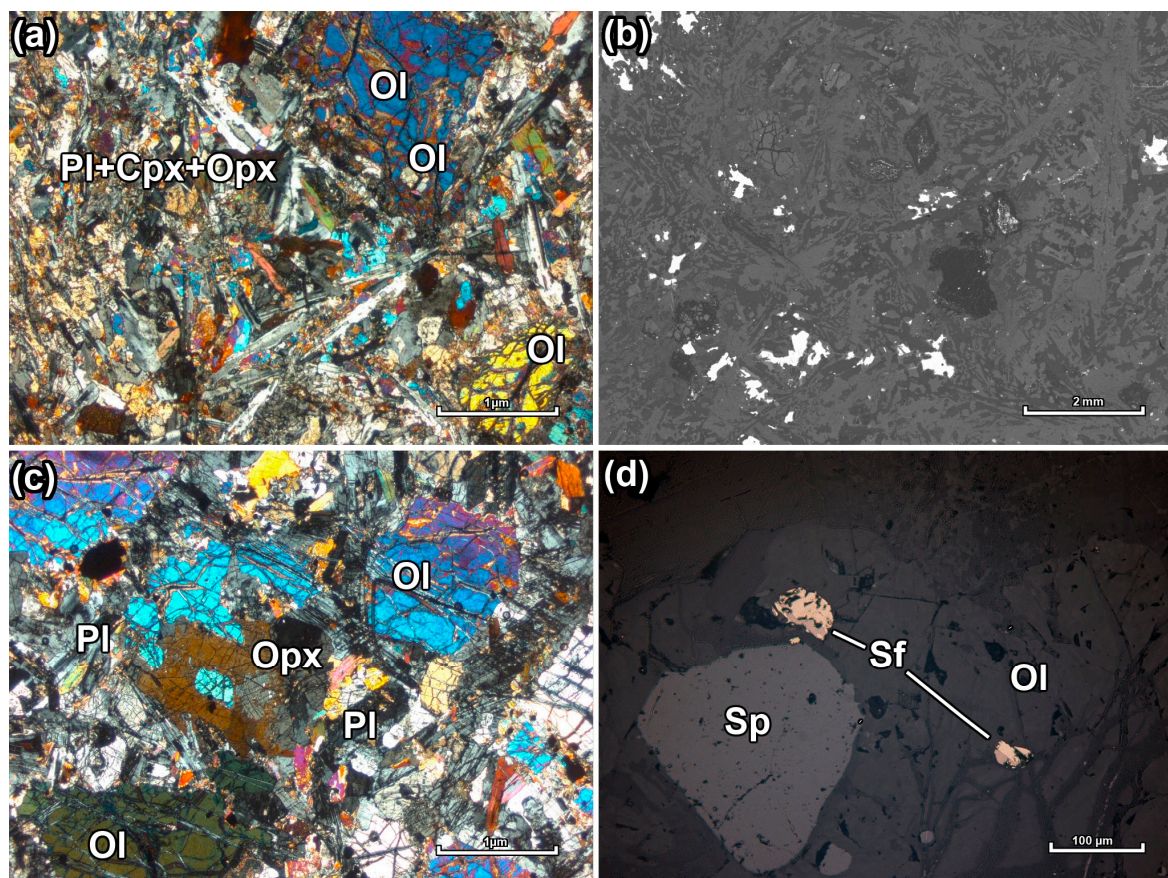


**Figure 2.** Textural features and mineral assemblages of chilled gabbronorite DV30-1 (a,b) and near-contact olivine gabbronorite DV30-4 (c,d) used in this study (Table 1). (a,c) Microphotographs of thin sections, (b) BSE image of a unique mount including disseminated sulfides, (d) image in reflected light presenting very rare, sometimes isometric sulfide grains.

### 2.1.2. Two Types of Plagioperidotite

Transition from the contact picrodolerite to the more ultramafic lithologies inward of the intrusive body is marked by the appearance of olivine gabbronorite (consistent with Ol-orthocumulate, Figure 2c,d) changed to melanocratic mesocumulates, referred to as ‘plagioclase peridotite’ or ‘plagioclase lherzolite’ [2,9]. These rocks compose a 150 m thick basal unit. In fact, these plagioperidotites represent a diversity of melanogabbronorite containing from ~30 vol% to ~70 vol% cumulus olivine. This transition is recorded in the transformation of the groundmass texture from ophitic to poikilitic, accompanied by an abrupt decrease in phlogopite (Figure 3a,b). Similar to the chilled gabbronorite and picrodolerite, only sparse separate grains of interstitial sulfides were observed (commonly less than 0.03–0.04 wt.% S or ~0.1 wt.% sulfide in the rock).

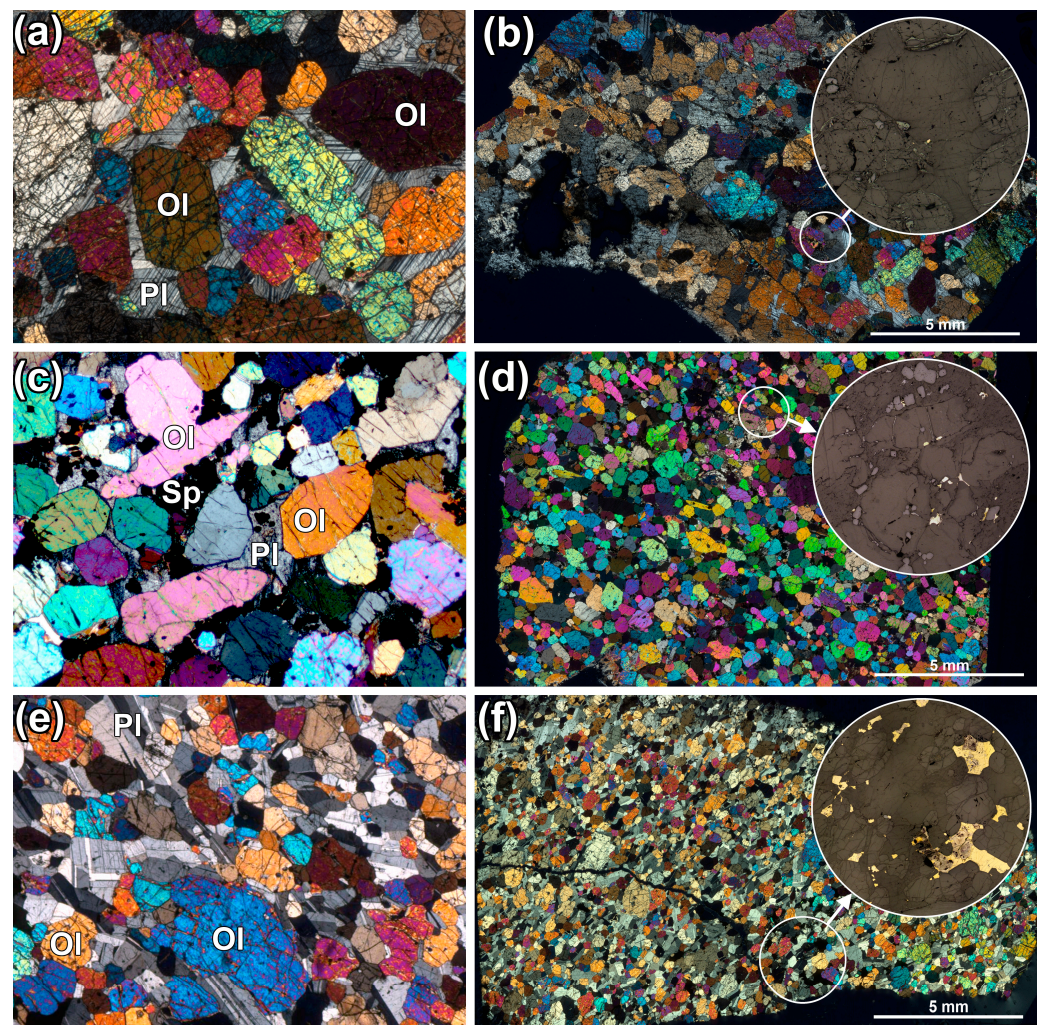


**Figure 3.** Textures of plagioperidotite 13DV547-16 (a,b), plagiodunite 13DV547-60 (c,d) and troctolite 13DV554-1 (e,f) used in this study (Table 1). (a,c,e) Microphotographs of thin sections, (b,d,f) images obtained by scanning thin sections using polarizing films. Inserts characterize sulfide-mineralized domains within these samples.

Despite the general textural and mineralogical similarity of the ultramafics, systematic differences in their chemical compositions allowed us to separate plagioperidotite into two principal types: the high-mg# Type I and the low-mg# Type II. This was achieved using the FeO-MgO diagram, where Type-I rocks display a linear trend towards the composition of olivine ~Fo88 (‘Fo88-trend’), whereas Type-II compositions extend towards olivine ~Fo86 (‘Fo86-trend’); see Figure 8 in [5]. Note that all samples of the picrodolerite from the

chilled margin and the lowermost olivine gabbro-norite are plotted together with Type-I plagioperidotite along the Fo88 trend.

### 2.1.3. Plagioclone and Pl-Containing Dunite

The plagioperidotite gradually transitions into a 50–60 m thick horizon of more magnesian plagioclone (Figure 3c,d), followed by a thick zone of adcumulate Pl-containing dunite (up to 970 m). Visually, differences between these two types of the most olivine-rich rocks are insignificant, however, in thin sections, plagioclone is readily distinguished from dunite by the amount of olivine (80–85 vol% vs. 90–97 vol%), wider distribution of poikilitic plagioclone, and irregular transformation of its texture from poikilitic to hypidiomorphic and then panidiomorphic. The latter is typical of almost monomineralic dunite at higher stratigraphic levels, where linear boundaries between olivine crystals, which meet at ~120° triple points, occur. This is accompanied by a systematic decrease in the proportion of intercumulus phases from 10–12 vol% to <5 vol% with very thin rims of pyroxene. In the lowest plagioclones, a horizon of poorly mineralized rocks is present.

### 2.1.4. Varieties of Troctolite

Upward, the dunite zone changes to a sequence of adcumulate melano- to leucotroctolites (~950 m), which contain minimum amounts of Cpx consistent with the very low porosity of the biminerallc Ol-Pl ( $\pm$  minor Sp) cumulate mixtures (Figure 1). In fact, this transition appears as an irregular zone ~100 m thick, marked by the first occurrence of intercalated layers of melanocratic troctolite and Pl-bearing dunite. Above this zone, the amount of troctolite, thickness of individual layers, and the amount of plagioclone in troctolite all generally increase, reaching their maximum in the uppermost troctolite. Most olivine crystals demonstrate a panidiomorphic granular texture (Figure 3e,f). Another feature of the troctolite unit is the appearance of Pl-rich agglomerations, observed as anorthositic schlieren, which are largest and most abundant near the irregular boundary of this zone with the overlying olivine gabbro. Petrological reconstructions suggest the entire troctolite succession locally experienced extreme gravitational separation and sorting of olivine and plagioclone [5]. Most troctolites are barren, containing only few small sulfide grains; however, in the lower half of the troctolite zone, some amounts of disseminated and locally PGE-rich sulfides were found (the so-called Konnikov zone [11], Figures 1 and 3f).

### 2.1.5. Olivine Gabbro and PGE-Mineralized Anorthosite

The uppermost portion of the troctolite unit represents a transitional zone composed of intercalated varieties of troctolite and olivine gabbro, as well as leucogabbro and gabbro-norite. Upward, the olivine gabbro becomes the major predominant type of cumulate forming a ~450 m thick zone (Figure 1). This is recorded in the marked increase in modal clinopyroxene, with the Cpx maximum observed at ~300 m above the formal contact with troctolite. A distinctive feature of the variable transition is the occurrence of numerous schlieren of anorthosite and veins of leucogabbro and gabbro-pegmatite with a taxitic texture. On average, the amount of the anorthositic schlieren decreases upwards, whereas veins of gabbro-pegmatite become more abundant. It is important that many of the anorthositic schlieren and lenses are PGE-mineralized, including patches of Cu-rich disseminated sulfides enriched in PGE [2,5–8,10].

### 2.1.6. Olivine Norite and Gabbro-norite

The unit of olivine gabbro changes to interbedding of olivine norite and olivine to Ol-free gabbro-norite (up to 600 m), with this heterogeneous sequence being transitioned to a 200 m thick horizon of the most evolved rocks, including pigeonite-containing gabbro and quartz–granophyre gabbro-norite near the roof of the intrusion. A thin unit of fine-grained chilled gabbro-norite comprises the upper endocontact of the YDM with hornfels (Figure 1). In fact, the gabbroic zone is extremely heterogeneous with numerous lenses of Pl-rich norite and gabbro-pegmatites, in some places demonstrating probable xenoliths

which seem to represent blocks of re-melted hornfels sunken from the roof [4]. Sulfide mineralization within the upper part of Dovyren is also variable, occurring as localized areas of disseminated sulfides. Herein, we note only one distinct lens of mineralized olivine-free and Pig-containing gabbro-norite enriched in disseminated sulfides (up to 6–9 wt.%), which was discovered in the Tsentralnyi cross section near the roof of the YDM [5].

## 2.2. Underlying Sills/Apophyses

In addition to the YDM, the Dovyren Intrusive Complex includes a number of mafic-ultramafic lenticular bodies (often referred to as ‘sills’), mostly 10 m to 200 m thick, which are generally sub-parallel to the lower contact of the intrusion [2,5,9]. Similar to the YDM, the underlying sills dip almost vertically, allowing for sampling of their complete cross-sections. Geological mapping has demonstrated that these sills are separated from the bottom of the YDM by beds of hornfels and siltstones. However, in some places, the small intrusive bodies cut through or are connected with the basal parts of the intrusion, allowing for their consideration as apophyses from the main body [12,13]. Numerous dykes of leucocratic gabbro-norite and olivine gabbro-norite are closely associated with these sills/apophyses, locally cutting them and the country rocks.

In this paper, we focus on the rocks from the highly mineralized DV10 apophysis, which extends for a distance of several kilometers SW of the Bolshoi cross section (Figure 1), being composed of Pl-peridotite (in fact, highly melanocratic olivine gabbro-norite) and locally reaching as much as 280 m thick. This bulge was sampled from its lower to the upper contact, including major types of sulfide ores and varieties of the mineralized rocks. Petrographic features of rocks hosting this mineralization correspond to olivine ortho- and mesocumulates, with only the exception of a chilled picrodolerite at the direct lower contact, which is characterized by an ophitic groundmass, similar to chilled olivine gabbro-norite from the YDM.

## 3. Sampled Mineralization and Methods

### 3.1. Samples from the YDM

In this paper, we examine five major types of the syngenetic sulfide mineralization that occurs through the stratigraphic succession of the Yoko–Dovyren massif. These types are represented by seven samples selected for geochemical and isotopic studies (Table 1). Samples DV30-1 and DV30-4 are (1) chilled gabbro-norite and (2) contact olivine gabbro-norite. Both rocks were sampled at a distance no more 5.4 m from the lower contact of the YDM and contain only few disseminated sulfides. Nevertheless, within sample DV30-1 (h = 0.4 m) a 1 cm size cluster of disseminated sulfides was found during its cutting for polished sections (Figure 2b). Samples 13DV547-16 and 13DV547-60 are (3) plagioclase peridotite and (4) poorly-mineralized plagioclase peridotite from a horizon above the plagioclase peridotite (Table 1, Figure 3a–d). The former sample is attributed to the high-mg# Type I of peridotite (see above), which seems to have been crystallized from sulfide-undersaturated magmas [5].

Sample 13DV547-60 was classified as low-mg# Type-II plagioclase peridotite, sampled in a poorly-mineralized horizon, which is marked by a 3–5-fold increase in the S content from the background values of 0.02–0.03 wt% to 0.09–0.14 wt%, reaching locally as much as 0.6 wt% S (consistent with ~2 wt.% sulfide). Such a subtle increase in the bulk sulfur is correlated with the increase in cumulus olivine and, based on the CT studies, the first occurrence of small blebs of sulfides [14]. We interpret these observations as a signature of the earliest accumulation of minor amounts of immiscible sulfides within the Dovyren chamber.

The sample 13DV554-1 was taken to characterize the geochemistry and Os isotopic composition of the highest part of the Konnikov zone, containing small amounts of PGE-rich sulfides (Figure 3e,f). Despite most troctolites are lacking disseminated sulfides, during detailed sampling of these rocks along the stream of the Tsentralnyi Creek we discovered a number of mineralized samples with Cu-rich sulfides and minor pentlandite, enriched in

Pd ( $91 \pm 84$  ppm,  $n = 7$ ; max 250 ppm). Further sampling of the troctolite unit, including discovered outcrops, revealed a site of weakly-altered mesocratic troctolite, which contained irregular distributed silicate-sulfide clusters and agglomerations, several cm to ~10 cm in diameter.

Samples AA06a-1 and AA06a-2 represent two fragments of PGE-rich anorthosite from a feldspar schlieren attributed to the main PGE reef of the YDM (Table 1, Figure 4). Such anorthositic bodies are usually a few cm to 1 m thick and extend for 2 to 5 m along the massif strike (rarely > 40 m long), forming a discontinuous sulfide-poor mineralized zone initially entitled Reef I and traced for over 20 km [2]. Despite the sulfide-poor character of the main reef, the total of PGE-bearing sulfides in the anorthosite may locally reach up to 3–5 vol%. Due to irregular distribution of sulfides, the total concentration of PGE + Au in the rock varies over the range 0.3–12.1 ppm at 0.006–0.710 wt.% Cu and 0.023–0.430 wt.% Ni [6]. As many as 35 PGE minerals have been described in these rocks [10].

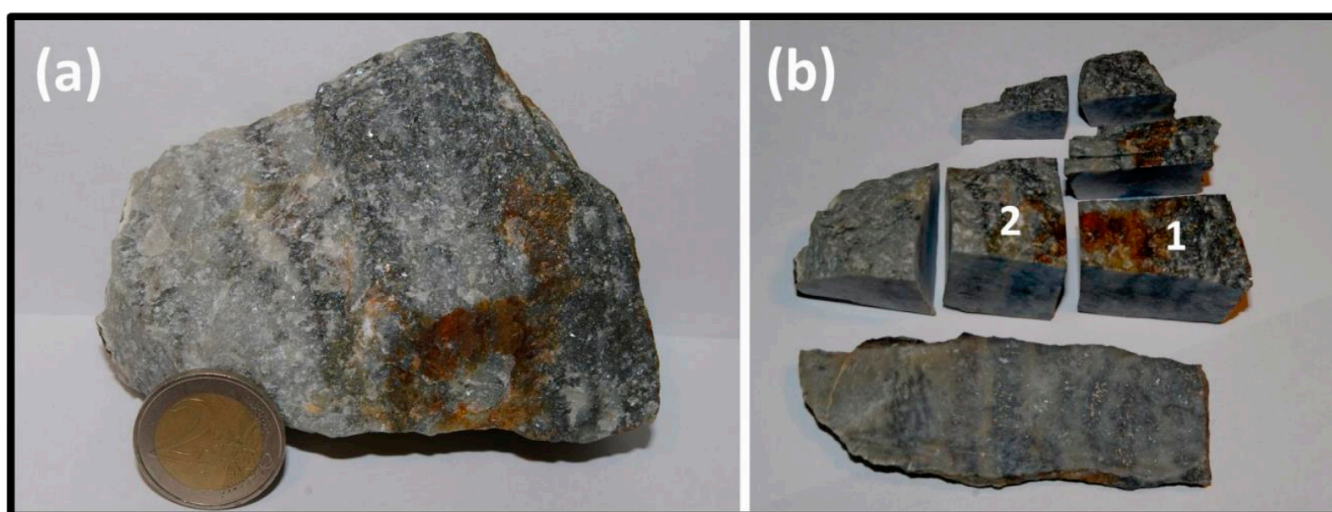


**Figure 4.** Low-mineralized PGE-rich anorthosite from sampling site 07DV146-1 within a large anorthositic schlieren of the main reef. (a) The initial sample from the 07DV146-1 outcrop, with darker domains and layers enriched in sulfide minerals, (b) fragments of its sawing used for additional analytical and isotopic studies: 1, AA06a-1; 2, AA06a-2. Small plates were used for preparation of thin sections.

### 3.2. Samples from the Apophysis DV10

Using results of microprobe studies and X-ray computed tomography, the diversity of sulfide-bearing rocks in the DV10 apophysis was subdivided into four types: (I) picrodolerite with droplet-shaped sulfides, (II) olivine gabbro-norite with sulfide morphology varying from rounded drops to irregular globules, (III) olivine gabbro-norite with larger globules and patchy net-textured sulfide domains, and (IV) the net-textured ores [12,13]. These varieties occur in the basal zone of this body, in the interval up to 30 m inward from the lower contact. (Figure 5) The observed sulfide assemblages including pyrrhotite, chalcopyrite, pentlandite, and cubanite occurred with slightly changing proportions, except for a relative decrease in the amount of chalcopyrite in the ore samples containing more than 5 vol% sulfides.

Three samples of types II, III, and IV from the highly mineralized area were selected for analyses, including globule-containing olivine gabbro-norite DV627-1-3, a fragment of net-textured ore DV625-2\_M, and globular ore DV628-2 (see 8–10 in Table 1).

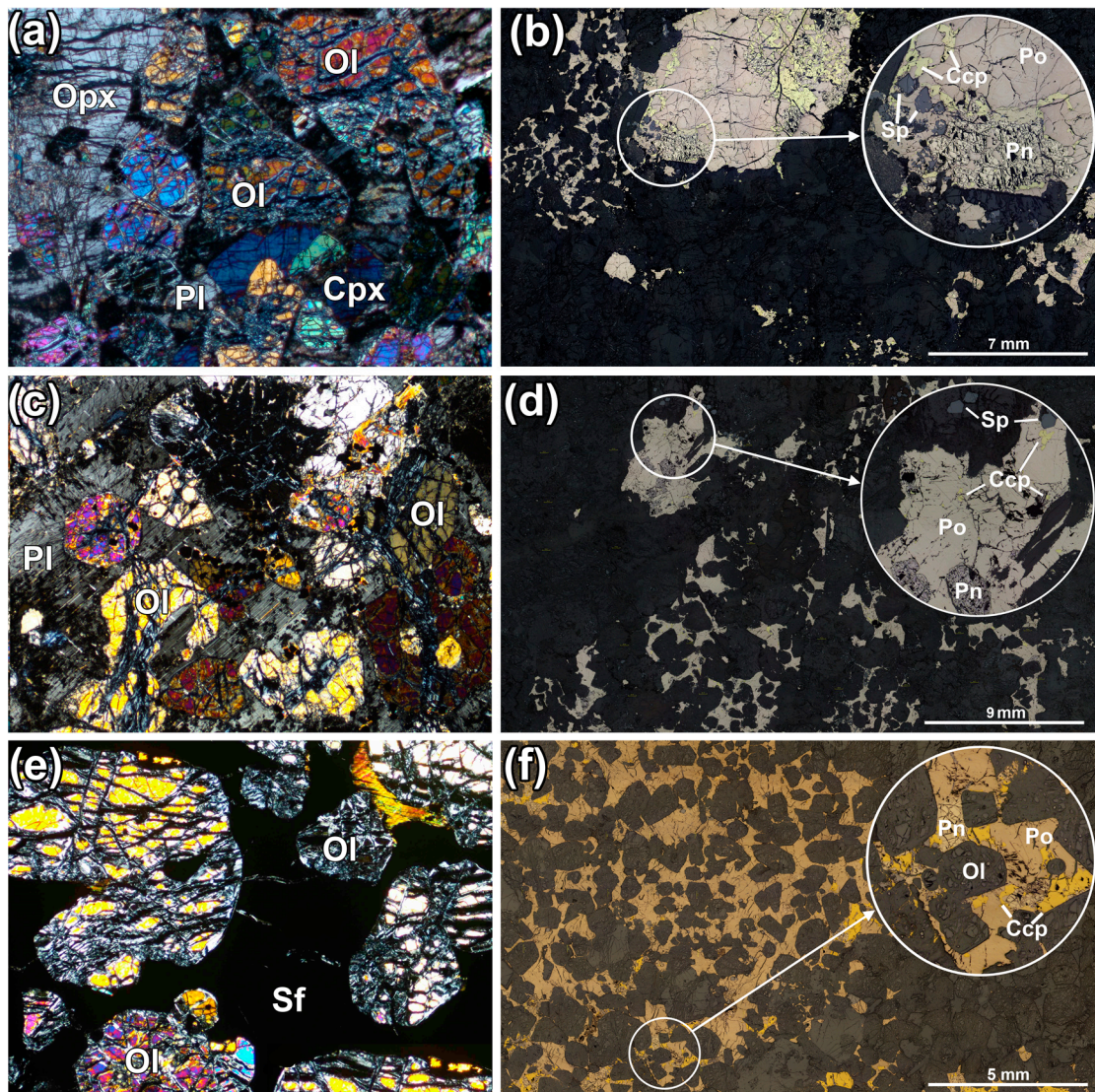


**Figure 5.** Microphotographs of highly mineralized samples from the DV10 apophysis used in this study (Figure 1, Table 1). (a,b) Olivine gabbro-norite DV627-1-3 with isolated sulfide globules, (c,d) net-textured ore DV625-2\_M, (e,f) globular ore DV628-2. (a,c,e) Microphotographs of thin sections, (b,d,f) images in reflected light. Inserts characterize sulfide-rich domains.

### 3.3. Analytical Studies

#### 3.3.1. Bulk Rock Compositions

The major elements and Cu for the YDM rocks were determined in GEOLABS (Sudbury, ON, Canada, <https://www.geologyontario.mndm.gov.on.ca/index.html>, accessed on 21 August 2023), whereas those from the ore-bearing DV10 apophysis were analyzed at the Laboratory for Analysis of Mineral Materials (IGEM, Russian Academy of Sciences, Moscow, Russia) using a conventional XRF technique with standard reference samples from the USGS. In the cases of the noble metals and most chalcophile elements we use a combination of methods from GEOLABS and the Laboratory of the Geochemistry and Analytical Chemistry of Noble Metals (Vernadsky Institute, Russian Academy of Sciences, Moscow, Russia). These details are given in [13]. Samples from the YDM were analyzed in the Canadian laboratory, for silver and gold using an ultra-trace ICP-MS method following an aqua regia digestion procedure (with detection limits 2–10 ppb for Ag and 0.4 ppb for Au). The concentrations of PGE were determined by ICPMS following fire-assay fusion (with ppb-detection limits 0.01 for Ir, 0.08 for Ru, 0.04 for Rh, 0.12 for Pd, and 0.17 for Pt).

Ore samples from the DV10 (Table 1) were analyzed at the Vernadsky Institute, starting from their decomposition by HF, HCl, and HNO<sub>3</sub> mixtures and followed by concentration of Au, Pt, and Pd on the POLYORGS IV adsorption agent. Then, these elements were analyzed via electrothermal atomic adsorption spectrometry (ETAAS) on a Solaar MQZ (ThermoElectron corporation, Waltham, MA, USA). Silver and some other elements were also determined via ETAAS. For the determinations, the ICP-MS-68B standard solution (A, B) was used (High-purity standards, Charleston, SC, USA), while the accuracy of these analyses was controlled by the SARM 7B certified reference material as 'Platinum ore' prepared by National Institute for Metallurgy and distributed by South African Bureau of Standards Reference Materials, Pretoria, Transvaal, South Africa).

### 3.3.2. Compositions of Rock-Forming Minerals

Most of the microprobe studies of mineral compositions were carried out using polished rock mounts and thin sections at the Laboratory of Local Methods of Studying Matter (the Faculty of Geology, Lomonosov MSU, Moscow, Russia). Three samples (DV30-1, DV30-2, and AA06-1) were analyzed in the Central Science Laboratory of the University of Tasmania (Hobart, Australia). In the first case, a JSM-6480LV electron microscope with a tungsten thermionic cathode (JEOL, Tokyo, Japan) equipped with an X-Max-N50 energy dispersive spectrometer (Oxford Instruments, Abingdon, Oxfordshire, UK) was used. An SX-100 electron microprobe was applied at the UTAS. Both standards and Dovyren samples were analyzed at an accelerating voltage of 20 kV and 10 nA at MSU and at 15 kV, 30 nA, and a beam size 2 μm (Ol) to 5 μm (Pl) at the UTAS.

To optimize the emission lines of characteristic radiation of elements, standard metal, stoichiometric oxide, and sulfide samples were used as references at MSU and the international standards USNM 115,900 (plagioclase LPL) and USNM 111,312/444 (San Carlos olivine) at the UTAS. Most of the averaged EMP analyses included from 5–7 (Pl) to 10–15 (Ol) individual spots.

### 3.3.3. Re-Os Isotope Studies

Os isotope and highly siderophile element concentration (HSE: Os, Ru, Ir, Pt, Re) data were obtained at the John de Laeter Centre, Curtin University (Perth, WA, Australia) using Carius tubes (CTs) to achieve complete digestion [15]. Approximately 0.2–0.3 g of rock powder was mixed with an appropriate amount of mixed <sup>185</sup>Re–<sup>190</sup>Os and HSEs spikes and was digested using concentrated acids (6 mL of purged double-distilled HNO<sub>3</sub> and 2 mL of triple-distilled HCl). This mixture was chilled and sealed in previously cleaned Pyrex™ borosilicate CT and heated to 220 °C for 60 h. Osmium was extracted from the acid solution using chloroform solvent extraction [16], then back extracted into HBr, followed by purification via micro distillation [17]. The purified Os was loaded onto Pt filaments and measured via negative thermal ionization mass spectrometry (TIMS) on a ThermoFisher Triton™ mass spectrometer using a secondary electron multiplier detector. The measured isotopic ratios were corrected for mass fractionation using <sup>192</sup>Os/<sup>188</sup>Os = 3.083.

Rhenium (and other HSEs) were separated via anion exchange chromatography, and Re, Ir, Ru, and Pt were measured using inductively coupled plasma mass spectrometry (ICPMS) coupled with a ThermoFisher ElementXR™ sector field ICP mass spectrometer. The HSE and Re-Os data are reported in Table 2. The measured UB-N reference material yielded an <sup>187</sup>Os/<sup>188</sup>Os ratio of  $0.1277 \pm 0.0003$ , agreeing with the reference value of  $0.1278 \pm 0.0002$ , and an Os concentration of  $3.58 \pm 0.10$  ppb, also in agreement with the reference value [18]. The AB-2 Os standard yielded an <sup>187</sup>Os/<sup>188</sup>Os ratio of  $0.10689 \pm 0.00022$  ( $n = 2$ ,  $2\sigma$  SD), which is consistent with reported values [19–23]. The total procedural blank for Os was 0.008 pg ( $n = 2$ ) and for Re was 12 pg. The <sup>187</sup>Os/<sup>188</sup>Os ratios for the blank were  $0.114 \pm 0.004$  ( $n = 2$ ). Since the total blanks for both Re and Os were run as part of each batch of dissolutions, the appropriate blank correction for each batch was applied.

**Table 2.** Petrochemical characteristics and concentrations of Re and PGE in selected rocks and sulfide ores of the YDM and Cu-Ni-PGE sulfide ores from the DV10 apophysis.

No	Sample	S, wt.%	Cr <sub>2</sub> O <sub>3</sub> , wt.%	Re, ppb	Os, ppb	Ir, ppb	Ru, ppb	Rh, ppb	Pd, ppb	Pt, ppb
1	DV30-1b	0.09	0.17	0.69	2.42	1.07	3.13	0.75	8.44	7.12
2	DV30-4b	0.06	0.69	0.49	15.3	8.42	28.2	3.94	22.4	18.2
3	13DV547-16	0.02	1.05	0.18	27.6	13.0	43.8	5.34	16.4	32.7
4	13DV547-60	0.06	2.75	0.98	22.3	12.8	49.9	19.0	39.0	59.5
5	13DV554-1	0.09	0.17	0.39	6.27	8.62	7.91	10.5	232	182
6	AA06a-1	1.47	0.007	8.17	3.00	13.0	6.89	25.3	2230	883
7	AA06a-2	1.08	0.008	7.56	8.10	33.5	16.8	88.2	2663	1663
8	DV627-1-3	0.54	0.56	3.30	8.71	-	-	-	231	65
9	DV625-2_M	11.5	0.43	0.98	1.66	-	-	-	2450	139
10	DV628-2	3.43	1.08	14.7	22.6	-	-	-	440	30
11	07DV107-1	9.11	0.43	-	-	10.7	15.7	36.0	913	133

Data for the net-textured ore 07DV107-1 are taken from the same outcrop as DV625-2\_M to be used for comparison in Figures 6 and 7.

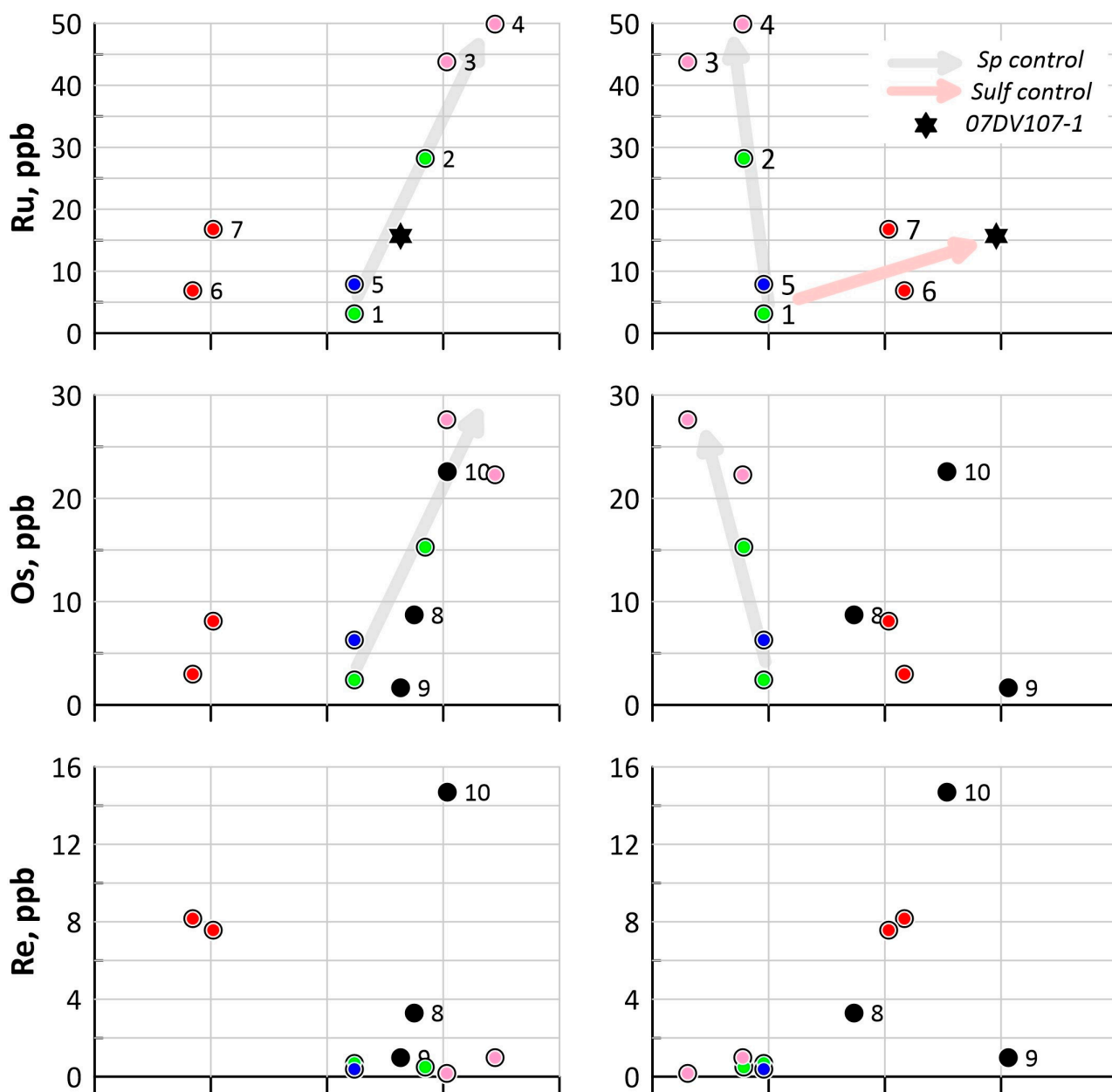


Figure 6. Cont.

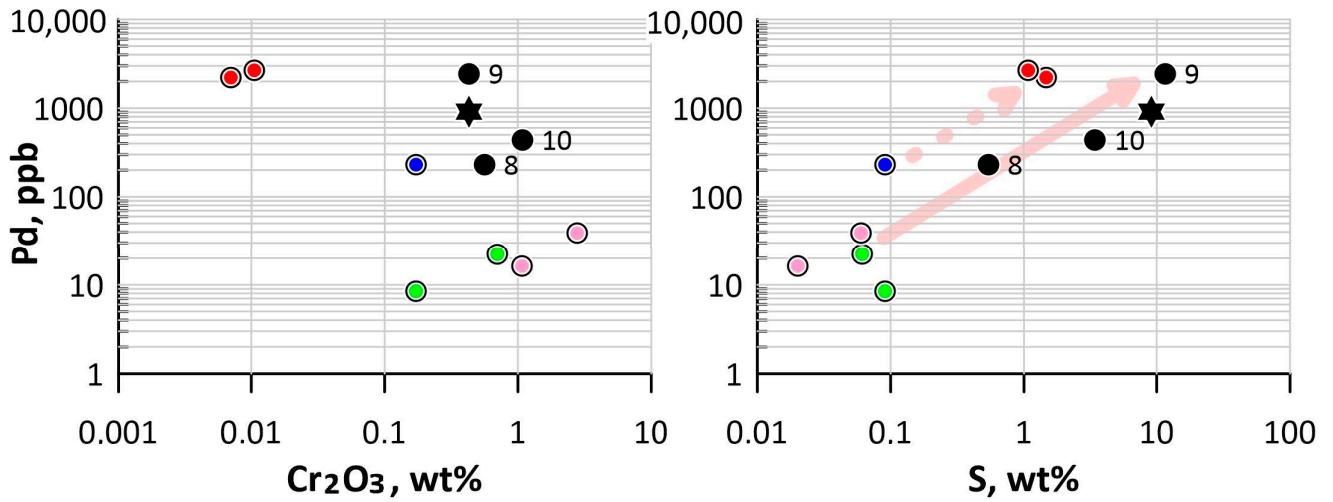


Figure 6. PGE and Re vs. Cr<sub>2</sub>O<sub>3</sub> and sulfur in the studied rocks. Numbers correspond to samples listed in Tables 1 and 2. Sample 07DV107-1 is a net-textured ore very similar to DV625-2\_M (point 9), see data for Pd. Data on Re and Os for 07DV107-1 are not available.

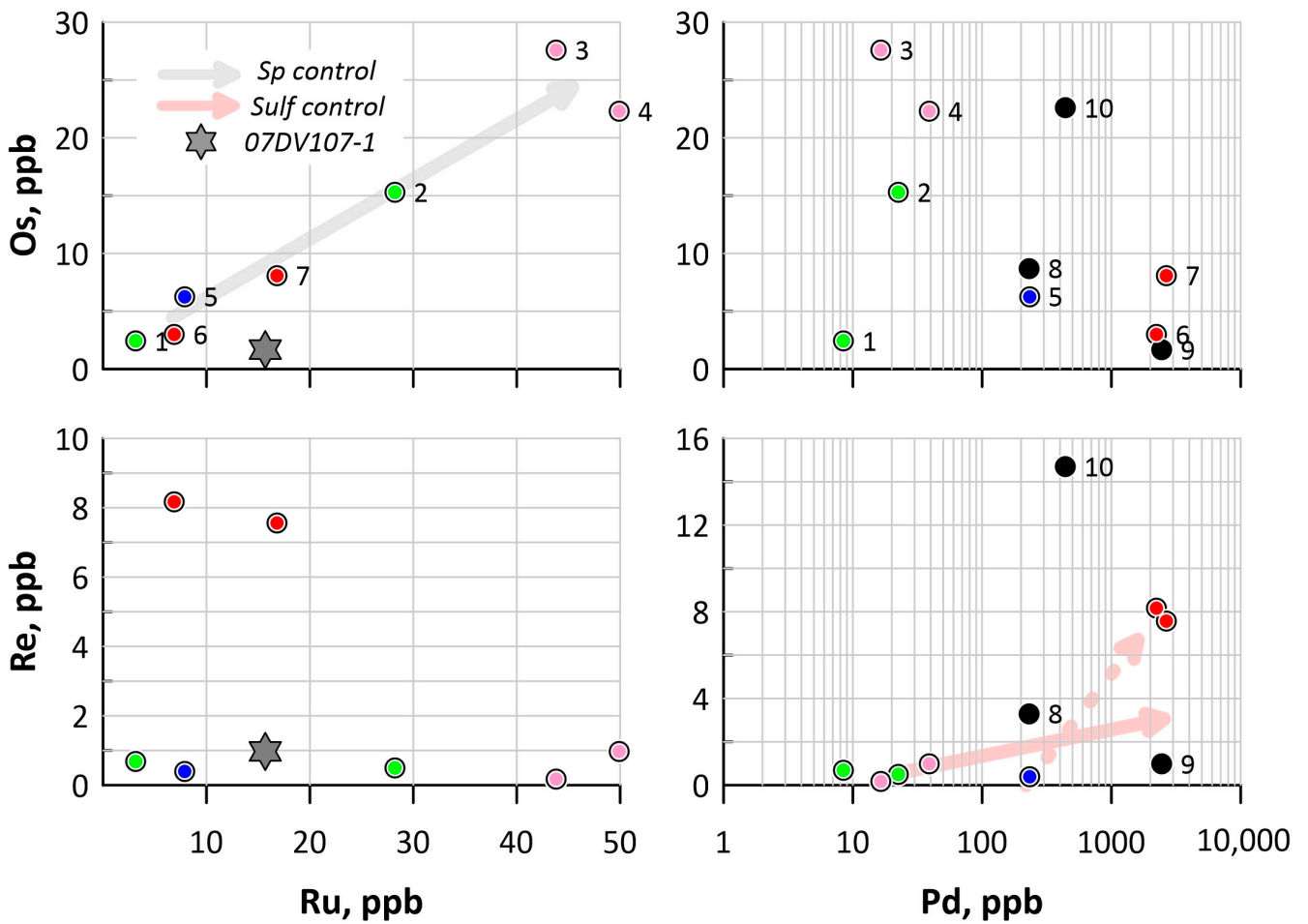


Figure 7. Correlations between whole-rock concentrations of Os, Re, Ru, and Pd in the examined samples. Designations follow Figure 6, except for 07DV107-1 for which Os and Re concentrations are approximated by data obtained for very similar net-textured ore DV625-2\_M (point 9 in Table 2).

## 4. Results

### 4.1. PGE-Geochemistry

The whole-rock concentrations of sulfur, Cr<sub>2</sub>O<sub>3</sub>, Re, and PGE are listed in Table 2. Genetically important correlations between these concentrations are summarized in Figures 6 and 7. Data in Figure 6 provide insight into the genetic diversity of the studied samples. Four plots to the left demonstrate the distinct “spinel control” of the behavior of Ru and Os, whereas those to the right show the effect of the sulfide accumulation, particularly for Pd and, probably, Re.

Overall, the plagioperidotite 13DV547-16 and plagiodunite 13DV547-60 are enriched in Os and Ru, positively correlating with Cr<sub>2</sub>O<sub>3</sub> in the rocks. In contrast, the highest concentrations of Pd and Pt were observed in the mineralized anorthosite (AA06a-1 and -2) and the most sulfide rich sample DV625-2\_M (Figure 6). In addition, note a two-fold increase in Pd and Pt in the plagiodunite compared with the plagioperidotite 13DV547-16 (Table 2), which is correlated with a subtle but principal ~three-fold increase in the sulfur. This spike is considered as a signature of the onset of sulfide immiscibility occurring in the Dovyren cumulates. This interpretation is supported by the results of the X-ray computed tomography, which indicate the first appearance of the small sulfide blebs in samples of plagiodunite, including 13DV547-60 [14].

In fact, following from these data, it is difficult to unambiguously specify the effect of sulfides on Os and Re partitioning, as the net-textured ore DV625-2\_M (point 9 in Figure 6) displays very low concentrations of both elements (Table 2). Another interesting feature is that points of Pd vs. S in the mineralized troctolite (point 5) and anorthosite (points 6–7) follow a sub-trend of markedly higher concentrations with respect to ultramafics and sulfide ore samples. This is consistent with more cuprous sulfide mineral assemblages observed in these rocks, compared with Mss-like sulfides from the basal zone of the YDM and ore samples from the DV10 [5,12,13].

The above speculations are supported by data from Figure 7, where correlations of Os and Re vs. Ru and Pd are shown. Ru is considered here as a marker of spinel control, whereas Pd is assumed to be indicator of the effect of accumulated sulfides. A distinct positive correlation between Os and Ru evidences their affinity to the spinel crystallization, with the absence of any positive correlation of Os with Pd. Re is inconsistent with the spinel-enriched ultramafics (see Re vs. Ru), demonstrating higher concentrations in Pd-rich (sulfide-enriched) rocks. The only (somewhat unusual) exclusion is the net-textured ore DV625-2\_M (point 9), which displays the lowest concentration of Re at the highest Pd.

### 4.2. Re-Os Isotope Systematics

The whole-rock Re and Os concentrations, the bulk Re/Os ratio, and <sup>187</sup>Re/<sup>188</sup>Os ratios together with <sup>187</sup>Os/<sup>188</sup>Os isotopic data are listed in Table 3 and shown in the isochron diagram (Figure 8a). Except for chilled gabbronorite DV30-1 from the lower contact of YDM, three samples from the basal zone and troctolite yielded the most primitive measured <sup>187</sup>Os/<sup>188</sup>Os compositions in the range 0.1293–0.1371, all with very low and similar <sup>187</sup>Re/<sup>188</sup>Os ratios (points 2–5, Table 3). Analysis of the chilled gabbronorite DV30-1 and near-contact olivine gabbronorite DV627-1-3 from the DV10 apophysis (black star in Figure 8) gave more radiogenic measured <sup>187</sup>Os/<sup>188</sup>Os compositions: 0.1519 and 0.1567, respectively. Two samples of sulfide ore, DV625-2\_M and DV628-2 from DV10, have slightly more radiogenic <sup>187</sup>Os/<sup>188</sup>Os isotopic composition, with <sup>187</sup>Os/<sup>188</sup>Os of 0.1678 and 0.1694, corresponding to points 9 and 10, respectively. Both pieces of PGE-mineralized anorthosite AA06a (Figure 4) display the most radiogenic characteristics, with measured <sup>187</sup>Os/<sup>188</sup>Os ranging from 0.1842 to 0.3032 and <sup>187</sup>Re/<sup>188</sup>Os from 4.532 to 13.43.

**Table 3.** Re and Os isotope composition of the examined Dovyren rocks and Cu-Ni-PGE sulfide ores.

Sample	Re (ppb)	Os (ppb)	Re/Os	$^{187}\text{Re}/^{188}\text{Os}$	$2\sigma$	$^{187}\text{Os}/^{188}\text{Os}$	$2\sigma$	$^{187}\text{Os}/^{188}\text{Os}(t)$	$2\sigma$	$\gamma\text{Os}(t)$	$2\sigma$
DV30-1b	0.69	2.42	0.2870	1.387	0.052	0.1519	0.0007	0.1350	0.0009	10.5	0.7
DV30-4b	0.49	15.32	0.0317	0.153	0.006	0.1295	0.0003	0.1276	0.0003	4.5	0.2
13DV547-16	0.18	27.64	0.0066	0.032	0.004	0.1293	0.0002	0.1289	0.0002	5.6	0.2
13DV547-60	0.98	22.99	0.0427	0.206	0.014	0.1353	0.0012	0.1328	0.0012	8.7	0.9
13DV554-1	0.39	6.27	0.0630	0.304	0.022	0.1371	0.0003	0.1334	0.0004	9.2	0.3
AA06a-1	8.17	3.00	2.7239	13.427	0.262	0.3032	0.0004	0.1393	0.0032	14.1	2.3
AA06a-2	7.56	8.10	0.9335	4.532	0.053	0.1842	0.0008	0.1289	0.0010	5.6	0.8
627-1-3	3.30	8.71	0.3789	1.833	0.021	0.1567	0.0004	0.1343	0.0004	10.0	0.3
625-2_M	0.98	1.66	0.5917	2.866	0.027	0.1678	0.0005	0.1328	0.0006	8.8	0.5
628-2	14.68	22.63	0.6487	3.143	0.034	0.1694	0.0002	0.1311	0.0005	7.3	0.4
Average								<b>0.1324</b>	<b>0.0035</b>	<b>8.4</b>	<b>2.9</b>

Initial  $^{187}\text{Os}/^{188}\text{Os}(t)$  and  $\gamma\text{Os}(t)$  are calculated for  $t = 728$  Ma, accepted as the age of the Dovyren Intrusive Complex [5].

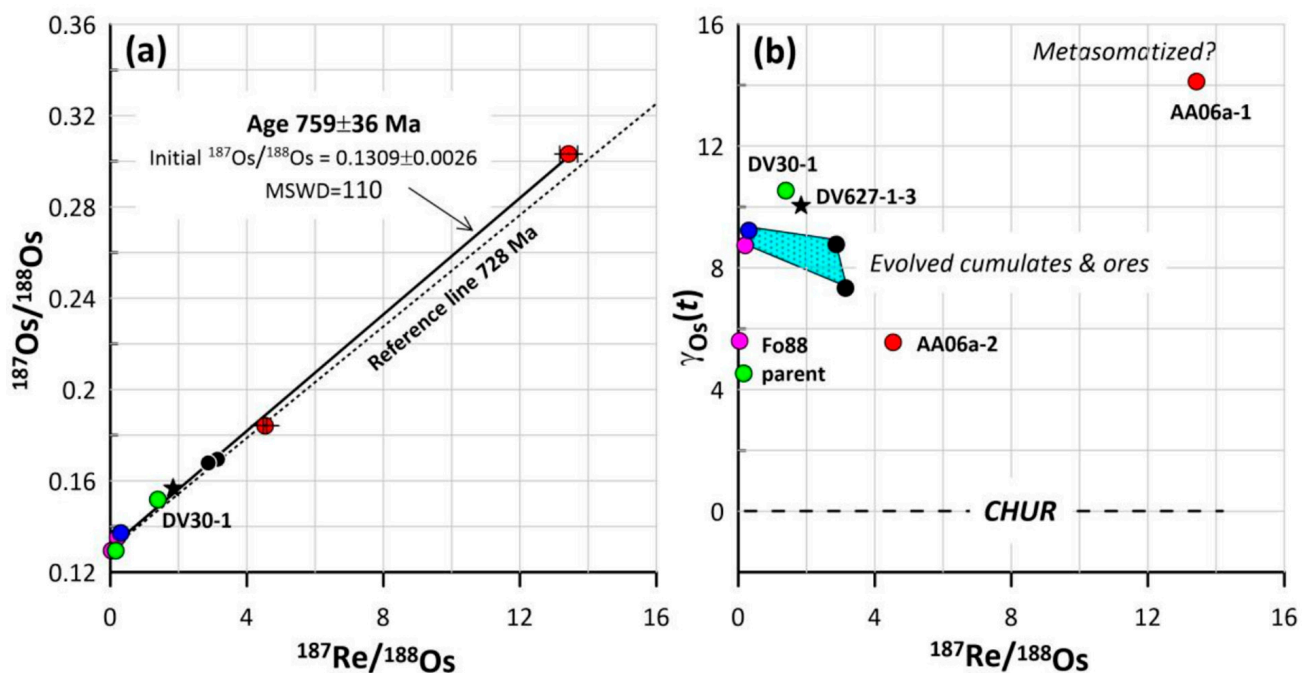


**Figure 8.**  $^{187}\text{Os}/^{188}\text{Os}$  vs.  $^{187}\text{Re}/^{188}\text{Os}$  isochron (a) and  $\gamma\text{Os}(t)$  vs.  $^{187}\text{Re}/^{188}\text{Os}$  at 728 Ma (b) for the examined Dovyren rocks. Designations follow Figures 6 and 7, except for the black star for the olivine gabbronorite DV627-1-3 (to separate this near-contact olivine gabbronorite from the sulfide ores in the DV10 apophysis). Reference line for age 728 Ma from U-Pb dating of zircon [5] was constructed assuming initial  $^{187}\text{Os}/^{188}\text{Os} = 0.13$ .

Despite the genetic diversity of the selected samples and accounting for the very high MSWD = 110 (probably due to a subtle but perceptible effect of overprinting processes, see Discussion), all data points show linear regression for  $759 \pm 36$  Ma with the initial  $^{187}\text{Os}/^{188}\text{Os}$  at  $0.1309 \pm 0.0026$  (Figure 8a). Within this uncertainty, this estimate is consistent with more precise results of U-Pb dating of zircon, which yielded the age  $731 \pm 4$  Ma for the 200 m thick Camel Sill underlying the YDM (5 samples) and  $728.4 \pm 3.4$  Ma (MSWD = 1.8, 11 samples,  $n = 99$ ) for the Dovyren Intrusive Complex, which includes both the YDM and underlying mafic to ultramafic sills/apophyses [5]. The 728 Ma reference isochron is shown in Figure 8a for comparison. The scatter on the isochron may be attributed to the variations in the initial Os ratios of the rocks, discussed in more detail below.

Another interesting feature of the obtained data (Table 3) is that being recalculated to  $\gamma\text{Os}(t)$  at  $t = 728$  Ma, they demonstrate three clusters in the  $\gamma\text{Os}(t) - ^{187}\text{Re}/^{188}\text{Os}$  coordinates (Figure 8b). The chilled and near-contact olivine gabbronorites DV30-1 (YDM) and DV627-1-3 (DV10) reveal the most radiogenic values  $\gamma\text{Os}(t)$   $10.5 \pm 0.7$  and  $10.0 \pm 0.3$  among the

basal ultramafics (Table 3, Figure 8b). Plagioclone 13DV547-60, troctolite 13DV554-1, and sulfide ores from the DV10 (9 and 10 in Table 1) yielded slightly lower but relatively radiogenic initial compositions, with  $\gamma_{Os}(t)$  ranging from  $7.3 \pm 0.4$  to  $8.7 \pm 0.9$ , whereas olivine gabbro-norite DV30-4 and plagioperidotite 13DV547-16 from the basal zone of the YDM (both belong to the Type-I rocks or the 'Fo88-trend'; see above) and PGE-rich anorthosite AA06a-2 yielded relatively primitive  $\gamma_{Os}(t)$  in the range 4.5–5.6 (on average  $5.2 \pm 0.6$ ).

## 5. Discussion

### 5.1. Processes Affecting Original Isotopic Characteristics

As seen from Table 3 and Figure 8a, the main input into the uncertainty of the Re-Os age comes from data on the AA06a-1 sample, which exhibits the highest measured  $^{187}\text{Re}/^{188}\text{Os}$  ratio of ~13.4. One could relate this to higher amounts of sulfides, comparing the whole-rock concentration of sulfur in this sample (1.47 wt.% S) with that of the adjacent AA06a-2 (1.08 wt.% S), Table 2. However, the observed difference in S is only 26 rel.% at similar Re concentrations, whereas the measured concentration of Os in AA06a-1 is almost three-fold lower compared with that in AA06a-2. We suggest that, despite the spatial proximity of these pieces of the same sample (Figure 4), the most sulfide-rich sublayer AA06a-1 experienced some sort of Os loss during final solidification. The effect of migrating fluids has been proposed to explain local variations observed in the PGE geochemistry of the mineralized anorthosites [6]. At this stage, we are not ready to speculate on the details of the process, but just note that the late-stage processes of the metasomatic nature could change the bulk Re/Os ratio and calculated original Re-Os isotopic characteristics (Table 3), even in the scale of centimeters.

Another important observation concerns the samples closest to the intrusive contacts (DV30-1 and DV627-1-3). Both represent the stratigraphically lowest rocks of the YDM and DV10 (Table 1), so their spatial proximity to the direct intrusive contacts allows one to assume the most effective contact interaction of their parental magmas with their surroundings, including, probably, some input of crustal rhenium. This may explain their most radiogenic values  $\gamma_{Os}(t)$  among the basal ultramafics (Table 3, Figure 8b). Following this logic, lower values of  $\gamma_{Os}(t)$  for 13DV547-60, 13DV554-1, and sulfide ores could be considered as a manifestation of the lower degrees of interaction with the host rocks. However, in the case of the plagioclone and troctolite (situated deeply inside the YDM), a better explanation suggests a partial contamination by crustal Os, which could proceed by large-scale assimilation of the hosting Riphean schists and metasandstones during magma emplacement, or by the interaction with the same sediments in deeper levels at a pre-intrusive stage.

The whole array of Re-Os data to a first approximation follows the 728 Ma isochron (Figure 8a), with olivine gabbro-norite DV30-4 and plagioperidotite 13DV547-16 being the ultramafics with the lowest  $\gamma_{Os}(t)$  consistent with the lowest measured  $^{187}\text{Re}/^{188}\text{Os}$  and  $^{187}\text{Os}/^{188}\text{Os}$  ratios (Table 2). For this reason, these rocks could be considered as the only two samples that have largely preserved their original Re-Os isotopic integrity, whereas the others have signatures of overprinting processes. As far as the olivine gabbro-norite and plagioperidotite belong to the Type-I rocks following the 'Fo88-trend' [5], the products of crystallization of the corresponding high-temperature and high-Mg magma provide the best constraints on the Os isotopic composition of the probable mantle source of the Dovyren magmas.

### 5.2. $\gamma_{Os}(t)$ vs. $\epsilon_{Nd}(t)$ Relationships as Petrologic Indicator

Previous detailed studies of the Sr-Nd-Pb isotope systems for the YDM and other rocks of the Dovyren Intrusive Complex have demonstrated extremely high ratios of radiogenic Sr and Pb isotopes and very low  $\epsilon_{Nd}(t)$  values, ranging from -16 to -13.5 [4,24]. These isotopic variations were interpreted to indicate that all of the intrusive rocks were derived from an isotopically anomalous source, whose protolith was formed in the Neoproterozoic era as a

heterogeneous mantle system with decreased Sm/Nd ratios, probably due to some sort of metasomatization or contamination by crustal material (“the first stage contamination” of the Dovyren precursor) [4,5]. This prehistory is recorded in the minimum  $\epsilon\text{Nd}(t = 728)$  values around  $-16$ , which were observed in the chilled gabbronorite, picrodolerite, and bottom olivine gabbronorite, as the products of crystallization of the most primitive high-Mg magmas (Type I or Fo88 parent) in the Upper Riphean. Overlying plagioperidotites, troctolites, and olivine gabbronorites show systematically higher  $\epsilon\text{Nd}(t)$  values in a slightly wider range, approximately from  $-14.5$  to  $-13.5$ , with the plagioperidotite attributed to Type II or the Fo86 parent. A similar range of  $\epsilon\text{Nd}(t)$  was found in mafic to ultramafic bodies underlying the main pluton, as well in associated low-Ti volcanics [4]. Data on the Re-Os isotope system for the examined rocks (Table 1) give an additional insight into the nature of these petrologic vs. isotopic relationships (Figure 9).

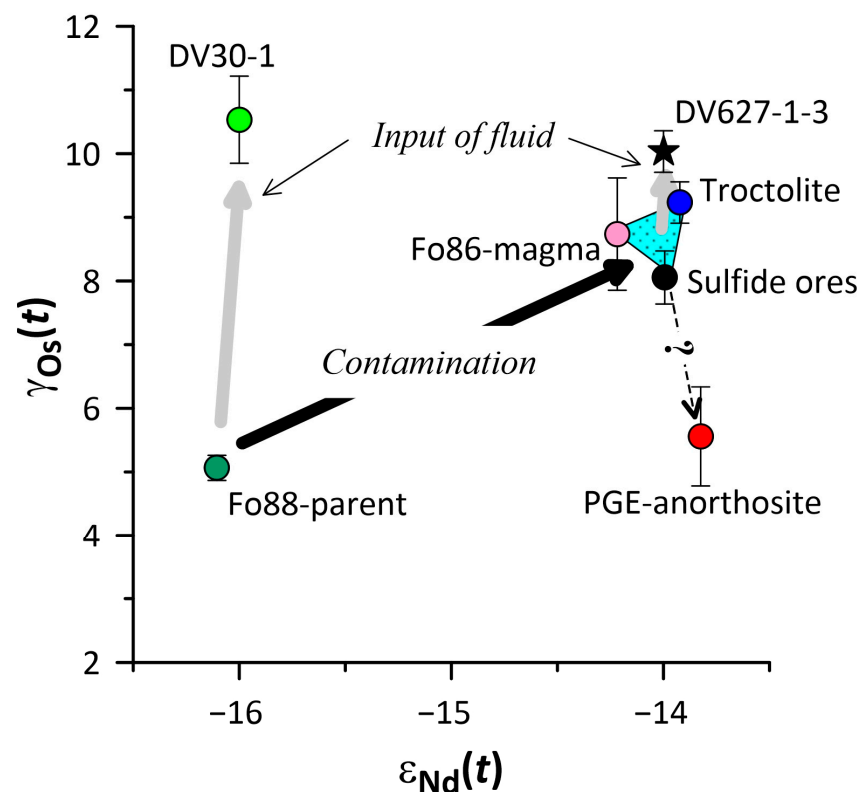


**Figure 9.** A petrologic–isotopic scheme demonstrating proposed genetic relations between probable Dovyren magmas (Fo88 and Fo86 parents) and isotopic characteristics of the main types of the examined rocks. Designations follow Figure 8, except  $\epsilon\text{Nd}(t = 728 \text{ Ma})$  values represent average estimates combining data from [24] with those from [1]; the error bars are not shown as they are smaller in size compared with the symbols in the diagram. For PGE-rich anorthosite, only data for AA06a-2 are shown, assuming its  $\epsilon\text{Nd}(t)$  to be the same as that in the hosting olivine gabbro [24].

Two primitive rocks with the lowest  $\epsilon\text{Nd}(t)$ , which were attributed to the Fo88 parent, demonstrate the lowest values of  $\gamma\text{Os}(t)$ , whereas other YDM rocks and mineralized olivine gabbronorites from the underlying sills/apophyses (with  $-14.5 < \epsilon\text{Nd}(t) < -13.5$ ) display systematically more evolved values  $\gamma\text{Os}(t)$ , Figure 9. These correlations may be considered as evidence that the initial Dovyren magma experienced interaction with hosting crustal materials in the Upper Riphean (“the second-stage contamination”), favoring an input of radiogenic osmium into the high-Mg parent and producing more evolved magma derivatives with slightly increased Sm/Nd ratio. Previous estimates argue that to increase  $\epsilon\text{Nd}(t)$  from  $-16$  to  $-14$ , initial high-Mg magma should assimilate  $\sim 10\%$  schists with

$\epsilon\text{Nd}(t) = -7$  from the terrigenous–carbonate sediments enclosing the YDM [4]. These genetic relations are shown in Figure 9 by the “Contamination” arrow.

In contrast, the chilled rocks from the YDM (chilled gabbronorite I2 in [24] and DV30-1 in this paper) have  $\epsilon\text{Nd}(t)$  values very similar to the proposed Fo88 parent, despite a marked difference in  $\gamma\text{Os}(t)$ , Figure 9. Similar relations are observed between the subcontact Ol-gabbronorite DV627-1-3 and overlying sulfide ores from the basal zone of the DV10 apophysis (see the gray sub-vertical arrows in Figure 9). These observations seem to indicate that both primitive and evolved Dovyren magmas did not follow additional whole-rock assimilation in situ, and instead experienced a local overprinting process, which could disturb their initial Re-Os isotopic systems.

This assumption is consistent with data on S isotopes demonstrating the highest values of  $\delta^{34}\text{S}$  in the chilled and subcontact rocks of both bodies (as much as +10–12), whereas data on higher stratigraphic levels yield much lower values around +2.5 [25,26]. For this particular case, it was proposed that the chilled and associated gabbronorites (more precisely, their magmatic precursors) were affected by a metamorphic  $\text{H}_2\text{S}$ -bearing fluid originating in the contact halo due to the thermal decomposition of pyrite in the host rocks (enriched in the  $^{34}\text{S}$  isotope) coupled with their dehydration [26].

We suggest that this process could disturb the initial Re-Os isotopic systems, enhancing the  $\gamma\text{Os}(t)$  value in the endocontact rocks of the Dovyren intrusive bodies. Unfortunately, the Re-Os isotopic data on the sedimentary pyrite from the Dovyren surroundings are absent. However, it is known that the crustal pyrite has highly radiogenic initial  $^{187}\text{Os}/^{188}\text{Os}$  isotopic composition [27,28], and both Re and Os are readily partitioned in fluid during high-temperature hydrothermal–metasomatic processes [29].

At this stage, it is difficult to interpret the very low  $\gamma\text{Os}(t) = +5.6 \pm 0.8$  observed in the PGE-rich anorthosite AA06a-2 (Table 3, Figures 8 and 9). Given that this rock has the same initial Os isotopic characteristics as recorded in the most primitive Dovyren magma, one should propose a petrologic process that could result in the formation of PGE-rich sulfide mineralized anorthosite with high  $^{187}\text{Re}/^{188}\text{Os} > 4.5$  from a gabbronoritic magma (Type II,  $^{187}\text{Re}/^{188}\text{Os} < 0.4$ ,  $\gamma\text{Os}(t) > 7.5$ ) without increase in the  $^{187}\text{Os}/^{188}\text{Os}(t)$  ratio (Table 3).

## 6. Conclusions

New data on PGE geochemistry and the Re-Os isotope system for 10 rocks from the Dovyren Intrusive Complex (Northern Transbaikalia, Russia) give rise to the following conclusions.

(1) Geochemical data for IPGE vs. PPGE allowed distinguishing between the “spinel” vs. “sulfide” control in the examined rocks, which is correlated with major magma types of the Dovyren Intrusive Complex, referred to as the high-temperature Fo88 parent and Fo86 parent, as well as their more evolved derivatives.

(2) Accounting for the very high MSWD = 110, all data points on the Re-Os isotope system yield the linear regression age of  $759 \pm 36$  Ma with the initial  $^{187}\text{Os}/^{188}\text{Os}$  at  $0.1309 \pm 0.0026$  (Figure 8a), possibly due to variations in the initial Os ratios related to the various degrees of contamination. This estimate is consistent with results of U-Pb dating of zircon, which yielded an age of  $728.4 \pm 3.4$  Ma for the Dovyren Intrusive Complex.

(3) It is shown that after recalculation to  $\gamma\text{Os}(t)$  at  $t = 728$  Ma, these isotopic compositions demonstrate three distinct clusters in the  $\gamma\text{Os}(t) - ^{187}\text{Re}/^{188}\text{Os}$  coordinates: (i) the chilled gabbronorite (YDM) and subcontact olivine gabbronorite (DV10) yielded the most radiogenic values of  $\gamma\text{Os}(t)$  10.5 and 10.0 among the basal ultramafics, (ii) plagioclone, troctolite, and sulfide ores showed lower radiogenic compositions, with  $\gamma\text{Os}(t)$  ranging from 7.3 to 8.7, (iii) olivine gabbronorite and plagioperidotite from the basal zone of the YDM and one sample of PGE-rich anorthosite yielded very primitive  $\gamma\text{Os}(t)$  in the range 4.5–5.6 (on average  $5.2 \pm 0.6$ ).

(4) Combining these Os isotopic characteristics with petrologic reconstructions and data on the Sm-Nd and sulfur isotope systems, the effect of the crust on the Dovyren magmatism and its mantle source can be divided into two stages. The first stage suggests

the Neoproterozoic origin of the mantle protolith with lowered Sm/Nd ratios compared with the primitive mantle [4,5], probably due to some sort of mantle–crust interaction. The second stage includes the Upper Riphean contamination of the most primitive Dovyren magma (Fo88 parent,  $\epsilon\text{Nd}(t)$  of  $-16$ ) by the hosting crustal rocks (probably of 10 wt% schists), generating more evolved Fo86-parent magma with higher  $\epsilon\text{Nd}(t)$  of  $-14$ . The occurrence of sulfide-mineralized rocks and Cu-Ni sulfide ores is related to this more evolved magma type.

(5) The highest values of  $\gamma\text{Os}(t)$  and relative enrichment in the  $^{34}\text{S}$  isotope in the chilled gabbro-norite (YDM) and subcontact olivine gabbro-norite (DV10) indicate that their Upper Riphean primitive to evolved magmatic precursors could be affected by a metamorphic fluid enriched in radiogenic  $^{187}\text{Os}$ , which originated in the exocontact halo due to the thermal decomposition of pyrite from the dehydrated country rocks.

(6) There is no obvious explanation for the relatively low  $\gamma\text{Os}(t) = +5.6 \pm 0.8$  observed in the PGE-rich anorthosite AA06a-2.

(7) The low values of  $\gamma\text{Os}(t)$  for the least fractionated rocks of the YDM suggest a primitive Upper Riphean mantle source with respect to the Os isotopic characteristics, which was extremely anomalous when considering the Sm-Nd isotope systematics for the same rocks with  $\epsilon\text{Nd}(t)$  around  $-16$ . Resolving this dilemma is a matter for the future.

**Author Contributions:** Conceptualization and methodology, A.A.A., S.G.T. and Y.A.K.; investigation (including field work), A.A.A., S.G.T., I.V.P., S.N.S., G.S.N. and E.V.K.; writing—original draft preparation, A.A.A.; writing—review and editing, S.G.T., Y.A.K., I.V.P. and E.V.K. All authors have read and agreed to the published version of the manuscript.

**Funding:** This study was supported by the Russian Science Foundation (grant No 23-77-01036).

**Data Availability Statement:** Not applicable.

**Acknowledgments:** Initial stages of this research were supported by projects FMUS-2019-0004 at the Vernadsky Institute of Geochemistry and Analytical Chemistry (RAS, Moscow, Russia) and AAAA-A21-121011390003-9 at the Dobretsov Geological Institute (SB RAS, Ulan-Ude, Russia). The authors thank Andrew W. McNeill (Mineral Resources Tasmania, Hobart, Australia) and Leonid V. Danyushevsky (University of Tasmania, Hobart, Australia) for their help during the 2007 field trip as well as some of the EPMA and XRF analyses. Marco Fiorentini (Centre for Exploration Targeting and the University of Western Australia, Perth, WA, Australia) kindly helped to manage isotope–geochemical studies, including PGE geochemistry of presented samples. We are grateful for the careful editing, suggestions, and constructive comments from three anonymous reviewers, promoting essential improvement of the finally submitted manuscript.

**Conflicts of Interest:** The authors declare no conflict of interest.

## References

1. Konnikov, E.G. *Differentiated Ultrabasic-Basic Complexes in the Precambrian Rocks of Transbaikalia*; Nauka: Novosibirsk, Russia, 1986; 127p. (In Russian)
2. Kislov, E.V. *The Yoko-Dovyren Layered Massif*; BNTs SD RAN: Ulan-Ude, Russia, 1998; 265p. (In Russian)
3. Polyakov, G.; Tolstykh, N.; Mekhonoshin, A.; Izokh, A.; Podlipkii, M.; Orsoev, D.; Kolotilina, T. Ultramafic–mafic igneous complexes of the Precambrian East Siberian metallogenic province (southern framing of the Siberian craton): Age, composition, origin, and ore potential. *Russ. Geol. Geophys.* **2013**, *54*, 1319–1331. [[CrossRef](#)]
4. Ariskin, A.A.; Danyushevsky, L.V.; Konnikov, E.G.; Maas, R.; Kostitsyn, Y.A.; McNeill, A.; Meffre, S.; Nikolaev, G.S.; Kislov, E.V. The Dovyren Intrusive Complex (Northern Baikal region, Russia): Isotope-geochemical markers of contamination of parental magmas and extreme enrichment of the source. *Russ. Geol. Geophys.* **2015**, *56*, 411–434. [[CrossRef](#)]
5. Ariskin, A.; Danyushevsky, L.; Nikolaev, G.; Kislov, E.; Fiorentini, M.; McNeill, A.; Kostitsyn, Y.; Goemann, K.; Feig, S.T.; Malyshev, A. The Dovyren Intrusive Complex (Southern Siberia, Russia): Insights into dynamics of an open magma chamber with implications for parental magma origin, composition, and Cu-Ni-PGE fertility. *Lithos* **2018**, *302–303*, 242–262. [[CrossRef](#)]
6. Konnikov, E.G.; Meurer, W.P.; Neruchev, S.S.; Prasolov, E.M.; Kislov, E.V.; Orsoev, D.A. Fluid Regime of platinum group elements (PGE) and gold-bearing reef formation in the Dovyren mafic–ultramafic layered complex, Eastern Siberia, Russia. *Miner. Depos.* **2000**, *35*, 526–532. [[CrossRef](#)]
7. Orsoev, D.A.; Rudashevsky, N.S.; Konnikov, E.G. Precious metal mineralization in low-sulfide ores of the Ioko–Dovyren layered massif, Northern Baikal region. *Trans. (Dokl.) Russ. Acad. Sci. (Earth Sci. Sect.)* **2003**, *390*, 545–549.

8. Tolstykh, N.D.; Orsoev, D.A.; Krivenko, A.P.; Izokh, A.E. *Noble-Metal Mineralization in Layered Ultrabasic–Basic Massifs of the Southern Siberian Platform*; Parallel': Novosibirsk, Russia, 2008; 194p. (In Russian)
9. Orsoev, D.A.; Mekhonoshin, A.S.; Kanakin, S.V.; Badmatsyrenova, R.A.; Khromova, E.A. Gabbro-peridotite sills of the Late Riphean Dovyren plutonic complex (Northern Baikal area, Russia). *Russ. Geol. Geophys.* **2018**, *59*, 472–485. [[CrossRef](#)]
10. Orsoev, D.A. Anorthosites of the low-sulfide platinumiferous horizon (Reef I) in the upper Riphean Yoko-Dovyren massif (Northern Cisbaikalia): New data on the composition, PGE–Cu–Ni mineralization, fluid regime, and formation conditions. *Geol. Ore Depos.* **2019**, *61*, 306–332. [[CrossRef](#)]
11. Ariskin, A.A.; Danyushevsky, L.V.; Fiorentini, M.; Nikolaev, G.S.; Kislov, E.V.; Pshenitsyn, I.V.; Yapaskurt, V.O.; Sobolev, S.N. Petrology, geochemistry, and the origin of sulfide-bearing and PGE-mineralized troctolites from the Konnikov Zone in the Yoko-Dovyren Layered Intrusion. *Russ. Geol. Geophys.* **2020**, *61*, 611–633. [[CrossRef](#)]
12. Pshenitsyn, I.V.; Ariskin, A.A.; Nikolaev, G.S.; Kislov, E.V.; Korost, D.V.; Yapaskurt, V.O.; Sobolev, S.N. Morphology, Mineralogy, and Composition of Sulfide Droplets in Picrodolerite from a Near-Bottom Apophysis of the Yoko-Dovyren Layered Intrusion. *Petrology* **2020**, *28*, 246–262. [[CrossRef](#)]
13. Pshenitsyn, I.V.; Ariskin, A.A.; Nikolaev, G.S.; Korost, D.V.; Yapaskurt, V.O.; Kislov, E.V.; Sobolev, S.N.; Kubrakova, I.V.; Tyutyunnik, O.A. Geochemistry and petrology of protosulfide melts in an ore-bearing apophysis of the Yoko-Dovyren intrusion. *Geochim. Int.* **2022**, *60*, 235–255. [[CrossRef](#)]
14. Korost, D.V.; Ariskin, A.A.; Pshenitsyn, I.V.; Khomyak, A.N. X-ray computed tomography as a method for reproducing 3D characteristics of sulfides and spinel disseminated in plagioclinites from the Yoko-Dovyren intrusion. *Petrology* **2019**, *27*, 370–385. [[CrossRef](#)]
15. Shirey, S.B.; Walker, R.J. Carius tube digestion for low-blank rhenium-osmium analysis. *Anal. Chem.* **1995**, *34*, 2136–2141. [[CrossRef](#)]
16. Cohen, A.S.; Waters, F.G. Separation of osmium from geological materials by solvent extraction for analysis by TIMS. *Anal. Chim. Acta* **1996**, *332*, 269–275. [[CrossRef](#)]
17. Birck, J.-L.; Roy-Barman, M.R.; Capmas, F. Re–Os isotopic measurements at the femtomole level in natural samples. *Geostand. News Lett.* **1997**, *20*, 19–27. [[CrossRef](#)]
18. Meisel, T.; Reisberg, L.; Moser, J.; Carignan, J.; Melcher, F.; Brüggmann, G. Re–Os systematics of UB–N, a serpentinized peridotite reference material. *Chem. Geol.* **2003**, *201*, 161–179. [[CrossRef](#)]
19. Aulbach, S.; Creaser, R.A.; Pearson, N.J.; Simonetti, S.S.; Heaman, L.M.; Griffin, W.L.; Stachel, T. Sulfide and whole rock Re–Os systematics of eclogite and pyroxenite xenoliths from the Slave Craton, Canada. *Earth Planet. Sci. Lett.* **2009**, *283*, 48–58. [[CrossRef](#)]
20. Azmy, K.; Kendall, B.; Creaser, R.A.; Heaman, L.; de Oliveira, T.F. Global correlation of the Vazante Group, São Francisco Basin, Brazil: Re–Os and U–Pb radiometric age constraints. *Precambrian Res.* **2008**, *164*, 160–172. [[CrossRef](#)]
21. Kendall, B.; Creaser, R.A.; Calver, C.R.; Raub, T.D.; Evans, D.A. Correlation of Sturtian diamictite successions in southern Australia and northwestern Tasmania by Re–Os black shale geochronology and the ambiguity of “Sturtian”-type diamictite–cap carbonate pairs as chronostratigraphic marker horizons. *Precambrian Res.* **2009**, *172*, 301–310. [[CrossRef](#)]
22. Rooney, A.D.; Selby, D.; Houzay, J.-P.; Renne, P.R. Re–Os geochronology of a Mesoproterozoic sedimentary succession, Taoudeni basin, Mauritania: Implications for basin-wide correlations and Re–Os organic-rich sediments systematics. *Earth Planet. Sci. Lett.* **2010**, *289*, 486–496. [[CrossRef](#)]
23. Tessalina, S.G.; Malitch, K.N.; Augé, T.; Puchkov, V.N.; Belousova, E.; McInnes, B.I. Origin of the Nizhny Tagil clinopyroxenite–dunite massif, Uralian platinum belt, Russia: Insights from PGE and Os isotope systematics. *J. Petrol.* **2015**, *56*, 2297–2318. [[CrossRef](#)]
24. Amelin, Y.; Neymark, L.; Ritsk, E.; Nemchin, A. Enriched Nd–Sr–Pb isotopic signatures in the Dovyren layered intrusion (Eastern Siberia, Russia): Evidence for source contamination by ancient upper-crust material. *Chem. Geol.* **1996**, *129*, 39–69. [[CrossRef](#)]
25. Grinenko, L.N. Sulfur Sources of Basic-Ultrabasic Rocks and Related Sulfide Copper–Nickel Ores. Ph.D. Thesis, GEOKhI RAN, Moscow, Russia, 1986; 292p. (In Russian)
26. Ariskin, A.A.; Pshenitsyn, I.V.; Dubinina, E.O.; Kossova, S.A.; Sobolev, S.N. Sulfur isotope composition of olivine gabbro-norites from a mineralized apophysis of the Yoko-Dovyren intrusion, Northern Transbaikalia, Russia. *Petrology* **2021**, *29*, 597–613. [[CrossRef](#)]
27. Lu, X.; Kendall, B.; Stein, H.J.; Hannah, J.L. Temporal record of osmium concentrations and  $^{187}\text{Os}/^{188}\text{Os}$  in organic-rich mudrocks: Implications for the osmium geochemical cycle and the use of osmium as a paleoceanographic tracer. *Geochim. Cosmochim. Acta* **2017**, *216*, 221–241. [[CrossRef](#)]
28. Saintilan, N.J.; Sproson, A.D.; Selby, D.; Rottier, B.; Casanova, V.; Creaser, R.A.; Kouzmanov, K.; Fontboté, L.; Piecha, M.; Gereke, M.; et al. Osmium isotopic constraints on sulphide formation in the epithermal environment of magmatic-hydrothermal mineral deposits. *Chem. Geol.* **2021**, *564*, 120053. [[CrossRef](#)]
29. Tessalina, S.G.; Yudovskaya, M.A.; Chaplygin, I.V.; Birck, J.-L.; Capmas, F. Sources of unique rhenium enrichment in fumaroles and sulphides at Kudryavy volcano. *Geochim. Cosmochim. Acta* **2008**, *72*, 889–909. [[CrossRef](#)]

**Disclaimer/Publisher’s Note:** The statements, opinions and data contained in all publications are solely those of the individual author(s) and contributor(s) and not of MDPI and/or the editor(s). MDPI and/or the editor(s) disclaim responsibility for any injury to people or property resulting from any ideas, methods, instructions or products referred to in the content.